

Channel-Aware Priority Transmission Scheme Using Joint Channel Estimation and Data Loading for OFDM Systems

Charles Pandana, Yan Sun, and K. J. Ray Liu, *Fellow, IEEE*

Abstract—This paper presents a data-loading technique that jointly considers the effect of channel estimation and the property of encoded multimedia data in Orthogonal Frequency Division Multiplexing (OFDM) systems. We observe that OFDM subchannels experience different average bit error rate (BER) due to channel estimation inaccuracy. The leakage effect in the fast Fourier transform (FFT)-based channel estimation method or the model mismatch in the polynomial-based channel estimation method results in a variation on the decoded BER across different OFDM subchannels. Thus, we are motivated to design the *Priority Transmission* (PT) scheme, which utilizes this BER variation across different OFDM subchannels and provides unequal error protection (UEP) for multimedia transmission. In addition, since OFDM has been adopted in many multimedia transmission standards, we compare the different channel estimation techniques, which were compared only for generic data transmission before, in the context of multimedia transmission with the PT scheme. In particular, we extend the polynomial-based channel estimation that was previously designed for a decision-directed scenario to a pilot-symbol-assisted (PSA) channel estimation scenario. Then, we investigate the channel estimation mean square error (MSE) and BER performance of individual OFDM subchannels for both the FFT-based and the polynomial-based channel estimation. Furthermore, we design the PT scheme that achieves significant gain in peak-signal-to-noise ratio (PSNR) of the reconstructed images for both channel estimation methods. Finally, we compare different OFDM channel estimation techniques for multimedia transmission. It is shown that for generic data transmission, the polynomial-based PSA channel estimation outperforms the FFT-based method in realistic channel conditions, and both types of channel estimation have similar performance when using the proposed PT scheme for multimedia transmission.

Index Terms—Channel estimation, priority transmission, unequal error protection, leakage effect, wireless multimedia transmission.

Manuscript received November 21, 2003; revised November 1, 2004. This work was supported in part by DAAD190120008. This paper was presented in part at the IEEE International Workshop on Multimedia Signal Processing (MMSP 02) and IEEE International Conference on Image Processing (ICIP 03). The associate editor coordinating the review of this manuscript and approving it for publication was Prof. Xiaodong Wang.

C. Pandana and K. J. R. Liu are with the Institute for System Research and Department of Electrical and Computer Engineering, University of Maryland, College Park, MD 20742 USA (e-mail: cpandana@glue.umd.edu; kjrlu@umd.edu).

Y. Sun was with the Institute for System Research and Department of Electrical and Computer Engineering, University of Maryland, College Park, MD 20742 USA. She is currently with the Electrical and Computer Engineering Department, University of Rhode Island, Kingston, RI 02881 USA (e-mail: yansun@ele.uri.edu).

Digital Object Identifier 10.1109/TSP.2005.851166

I. INTRODUCTION

WIRELESS multimedia services that require high data rate transmission have become a major driving force in the development of broadband wireless communications. Many high-speed wireless transmission standards, such as digital audio broadcasting (DAB) [1], digital video broadcasting (DVB-T) [2], and broadband wireless LAN (IEEE 802.11a) [3], adopt Orthogonal Frequency Division Multiplexing (OFDM) modulation, which is known for its advantages of transforming frequency-selective fading channels into a set of parallel flat fading subchannels and eliminating intersymbol interference (ISI) [4], [5].

In OFDM systems, *channel estimation* is crucial for coherent demodulation and has a significant impact on overall performance [6]–[8]. Previous channel estimation techniques mainly concern the transmission of generic data and focus on reducing the average estimation errors [6], [7]. Since multimedia data will contribute a large proportion of the traffic in high-speed wireless communications, it is important to understand how the channel estimation can effect the multimedia transmission.

An important class of channel estimation techniques is pilot-symbol-assisted (PSA) channel estimation, which estimates OFDM channel based on a set of training symbols inserted into data streams and is suggested by many standards [2], [3]. Most PSA channel estimation schemes use the Fast Fourier Transform (FFT) to reduce noise and estimate the subchannels that do not transmit training pilots, as in [9] and [10]. However, the FFT-based channel estimation suffers from the *leakage effect* when the delay paths are not separated by integer multiples of the system sampling period [6]–[8]. The main consequence of the leakage effect is that the OFDM subchannels experience nonuniform average estimation error. As a result, there exists a variation on decoded bit error rate (BER) across different subchannels. This BER variation is highly undesirable for generic data transmission because the worst subchannels dominate the error performance. For the multimedia transmission, however, we can utilize the leakage effect to provide unequal error protection (UEP). In particular, we design a *Priority Transmission* (PT) scheme that loads multimedia data to OFDM subchannels according to the importance of the data and the channel estimation error with the decoding delay constraint [11], [12]. The PT scheme is suitable for a variety of compressed multimedia data. In this paper, we use Set Partitioning in Hierarchical Trees (SPIHT) [13] encoded images to demonstrate the performance of the PT. We

show that the PT scheme significantly improves the quality of the reconstructed images, compared with the schemes that do not exploit the channel estimation.

Another way to combat the leakage effect is to use polynomial-based channel estimation techniques [14]–[16], which use polynomial basis functions to replace the exponential basis functions used in the FFT-based methods. The polynomial-based methods were originally proposed for decision-directed channel estimation schemes and do not suffer from the leakage effect [15]. In order to fully understand the effects of the PT scheme on different channel estimation methods, we develop the polynomial-based PSA channel estimation, where we observe the variation of BER across subchannels. Therefore, the PT can also be applied to the polynomial-based PSA methods. Moreover, we show that the FFT-based method is effective in interpolating the sinusoidal like function, whereas the polynomial-based method performs well as long as the channel varies smoothly in one interpolation window.

Previously, channel estimation techniques were compared for their average BER performance, which makes perfect sense for the data transmission but not for multimedia. Therefore, the development of the PT scheme raises an interesting question on what channel estimation scheme is good for multimedia transmission. In this paper, we first extend the development of polynomial-based channel estimation in [16] to the polynomial-based PSA channel estimation. We also show that the polynomial-based PSA channel estimation outperforms the FFT-based method for data transmission in most realistic channel conditions. Moreover, for multimedia transmission, the polynomial-based PSA channel estimation is superior to the FFT-based method when PT is not used, and both channel estimation schemes achieve similar good performance when the PT scheme is employed.

The rest of the paper is organized as follows. Section II introduces the system description. We develop the polynomial-based PSA channel estimation method and design the PT scheme based on the derived channel estimation MSE for individual subchannel in Section III. In Section IV, the PT scheme is designed for the FFT-based channel estimation. The polynomial- and the FFT-based channel estimation techniques are compared in Section V for both generic data and multimedia transmission. Finally, conclusions are drawn in Section VI.

II. SYSTEM DESCRIPTION

In this section, we introduce the transmission systems, channel model, and the PSA channel estimation for OFDM systems. In addition, we summarize the properties of the SPIHT image codec to be used in our simulation.

A. OFDM System

Fig. 1 illustrates a high-level diagram of an OFDM system [15]. At the transmitter, input signals are arranged into blocks by a serial-to-parallel (S/P) converter, and the data in each block are mapped into a set of complex constellation points, i.e., $\{X[0, k], \dots, X[N-1, k]\}$. The mapped data block is often referred to as an OFDM block. Here, N is the total number

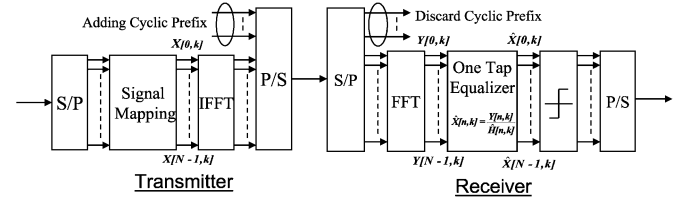


Fig. 1. Typical OFDM systems.

of subchannels, and k denotes the index of the OFDM blocks. After signal mapping, the modulation is implemented using inverse fast Fourier transform (IFFT). A cyclic prefix is then inserted to eliminate inter-symbol-interference (ISI). Finally, the modulated data block and the cyclic prefix are converted to an OFDM symbol by a parallel-to-serial (P/S) converter.

At the receiver, the cyclic prefix is discarded, and demodulation is performed by fast Fourier transform (FFT). When the length of the cyclic prefix is longer than the length of the channel impulse response, the interference between two consecutive OFDM symbols is eliminated. In this case, the channel can be viewed as a set of parallel independent subchannels, and the received signal is represented as

$$Y[n, k] = H[n, k]X[n, k] + w[n, k], \quad n = 0, \dots, N-1 \quad (1)$$

where $Y[n, k]$ represents the received signal, $X[n, k]$ denotes the transmitted signal, and $H[n, k]$ and $w[n, k]$ are the channel frequency response and the additive Gaussian noise, respectively. Here, n is the index of subchannels, and k is the index of OFDM blocks. The channel noise samples $\{w[n, k]\}$ are modeled as Gaussian random variables with zero mean and variance σ^2 and are assumed to be independent for different n 's or k 's [7], [16], [17].

In addition, the receiver performs channel estimation and obtains the estimated channel frequency response, which is denoted by $\hat{H}[n, k]$. Finally, the receiver produces the estimated transmitted signal, which is denoted by $\hat{X}[n, k]$ using a one-tap equalizer as

$$\hat{X}[n, k] = \frac{\hat{H}^*[n, k]Y[n, k]}{|\hat{H}[n, k]|^2}. \quad (2)$$

B. Channel Model

In mobile wireless communication systems, signal transmission suffers from various impairments such as frequency-selective fading due to multipath delay [18]. As in [18] and [19], the complex baseband representation of wireless channel impulse response is expressed as

$$h(t, \tau) = \sum_i \gamma_i(t) \delta(\tau - \tau_i) \quad (3)$$

where $\gamma_i(t)$ and τ_i are the gain and the delay of the i th path, respectively. In Rayleigh fading, the sequence $\{\gamma_i(t)\}$ is modeled as zero-mean circular symmetric complex Gaussian random variable with variance σ_i^2 and is assumed to be independent for different paths [18], [19].

The channel frequency responses of OFDM subchannels can be approximated by the samples of the continuous channel frequency response [7], that is

$$\begin{aligned} H[n, k] &= \int_{-\infty}^{\infty} h(t, \tau) e^{-j2\pi f\tau} d\tau \Big|_{f=n\Delta f, t=kT_f} \\ &= \sum_i \gamma_i(kT_f) e^{-j2\pi n\Delta f\tau_i} \end{aligned} \quad (4)$$

where T_f is the duration of an OFDM symbol, $\Delta f = B_d/N$ is the bandwidth of each subchannel, and B_d is the total bandwidth. This approximation does not consider the effect of the smoothing filter at the transmitter and the front-end filter at the receiver.

The correlation function of the channel frequency response is usually simplified as the multiplication of time correlation and frequency correlation [7], [10], i.e.,

$$r_H[\Delta n, \Delta k] = r_f[\Delta n] r_t[\Delta k] \quad (5)$$

where the frequency correlation $r_f[\Delta n]$ can be expressed as

$$r_f[\Delta n] = \sum_i \frac{\sigma_i^2}{\sum_j \sigma_j^2} e^{-j2\pi\Delta n\Delta f\tau_i}. \quad (6)$$

Based on Jakes' model [20], the time correlation $r_t[\Delta k]$ can be expressed as

$$r_t[\Delta k] = J_0(2\pi T_f f_D \Delta k) \quad (7)$$

where $J_0(x)$ is the zeroth-order Bessel function of the first kind, and $f_D = (vf_c)/c$ is the Doppler frequency calculated from vehicle speed v , carrier frequency f_c , and the speed of light c .

C. Overview of Pilot-Symbol-Assisted (PSA) Channel Estimation

In PSA channel estimation, a set of predefined pilot symbols is inserted into the data streams to assist the channel estimation process [10], [17], [21], [22]. Let n_p and k_p denote the locations of the subchannels and the OFDM blocks, respectively, where the pilot symbols are transmitted. The PSA channel estimation usually consists of two steps. First, the receiver estimates the channel frequency response at the pilot locations as

$$\hat{H}[n_p, k_p] = \frac{Y[n_p, k_p]}{X[n_p, k_p]} = H[n_p, k_p] + w'[n_p, k_p] \quad (8)$$

where $w'[n_p, k_p] = (w[n_p, k_p])/(X[n_p, k_p])$ is the noise term, and $\hat{H}[n_p, k_p]$ is often referred to as the *temporal estimate*. Second, the channel responses of all subchannels are calculated from the temporal estimates through interpolation or filtering [10], [22]. The interpolation is typically applied both across subchannels in one OFDM block and across different OFDM blocks [9]. In this paper, we denote the pilot spacing along different subchannels and OFDM blocks as I_p and K_p , respectively. For instance, the pilot configuration shown in Fig. 2 corresponds to $I_p = 4$ and $K_p = 4$.

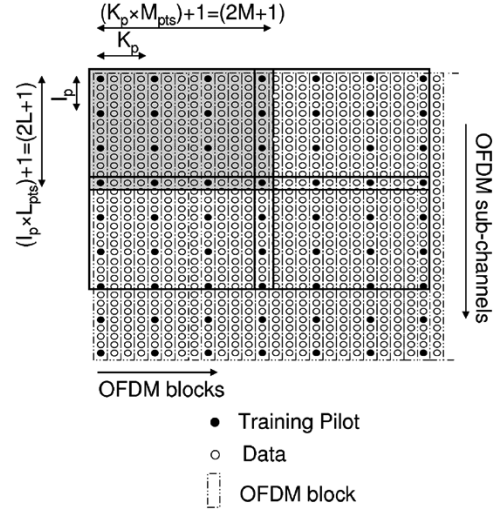


Fig. 2. Example of pilot symbol configuration.

D. Set Partitioning in Hierarchical Trees (SPIHT)

SPIHT [13] is a wavelet-based image compression technique that uses set partitioning hierarchical trees encoding. In SPIHT, the wavelet coefficients of the image are encoded using bit planes, and two passes are performed on each bit-plane. The first pass is the *sorting pass*, which determines the sign values and implicit location information of significant wavelet coefficients. The second pass is the *refinement pass*, which refines bit values of the significant coefficients [13]. Several important properties of SPIHT are summarized as follows: First, the SPIHT has a good rate-distortion performance for still images with comparatively low complexity. Second, it is scalable or completely embeddable, that is, the decoding algorithm can be stopped at any received bit. This scalable property is very suitable for image transmission. The transmitted image can be decoded until the first irrecoverable error occurs. The more bits that are received, the better quality the reconstructed image will have. Third, the encoded SPIHT bitstreams have the property that the later encoded bits are approximately less important than the earlier encoded bits. Due to this property, several unequal error protection (UEP) schemes [23], [24] based on forward error correcting (FEC) codes have been proposed. Those approaches generally apply stronger FEC codes to the more important portions of the SPIHT bitstreams. The method proposed in this paper utilizes this property in a different way. Instead of applying the stronger FEC to the more important bitstream, the PT scheme utilizes the best channel within the acceptable delay to transmit the most important data.

III. PRIORITY TRANSMISSION FOR POLYNOMIAL-BASED CHANNEL ESTIMATION

Due to the advantages of the PSA methods in the fast fading environment, we first extend the derivation in [16] and develop the polynomial-based PSA channel estimation scheme. We derive the channel estimation MSE and the decoded BER for different OFDM subchannels, and finally, we propose the PT scheme to improve the reliability of multimedia transmission

in OFDM systems using polynomial-based PSA channel estimation.

A. PSA Polynomial Channel Estimation: Algorithm Description

A time-varying wireless channel response can be approximated by a set of piecewise polynomial basis functions [25]. Let (n, k) denote the n th subchannel in the k th OFDM block. In a time-frequency window that has dimension $(2L+1) \times (2M+1)$ and is centered at (n_0, k_0) , the channel frequency response can be expressed as [15], [25]

$$H[n, k] = \sum_{i=0}^{I_{\text{deg}}} \sum_{j=0}^{J_{\text{deg}}} C_{n_0, k_0}[i, j] (n - n_0)^i (k - k_0)^j + S_{I_{\text{deg}} J_{\text{deg}}}[n, k] \quad \text{for } n_0 - L \leq n \leq n_0 + L, \text{ and } k_0 - M \leq k \leq k_0 + M \quad (9)$$

where I_{deg} and J_{deg} are the orders of the polynomial basis at frequency and time domain, respectively, $C_{n_0, k_0}[i, j]$ are the polynomial coefficients, and $S_{I_{\text{deg}} J_{\text{deg}}}[n, k]$ are the model errors. When the model errors are small (negligible), the channel can be fully described by the polynomial coefficients $C_{n_0, k_0}[i, j]$. Thus, the task of channel estimation is to obtain $C_{n_0, k_0}[i, j]$ from temporal estimation $\hat{H}[n_p, k_p]$ and estimate $H[n, k]$ through the two-dimensional (2-D) polynomial interpolation, as in (9).

In the following, we describe the polynomial-based PSA channel estimation with rectangular pilot symbol arrangement, as shown in Fig. 2. Without loss generality, we focus on the channel responses in the window that has size $(2L+1) \times (2M+1)$ and is centered at (L, M) . This window locates at the top-left corner of the pilot arrangement pattern in Fig. 2. The number of pilot symbols inside this window are $L_{\text{pts}} \times M_{\text{pts}}$, where $L_{\text{pts}} = \lceil (2L+1)/(I_p) \rceil$ and $M_{\text{pts}} = \lceil (2M+1)/(K_p) \rceil$. Recall that I_p and K_p denote the pilot spacing at the frequency and time domain, respectively. In addition, these pilot symbols are located at positions $(a \cdot I_p, b \cdot K_p)$, where $a = 0, 1, \dots, L_{\text{pts}} - 1$ and $b = 0, 1, \dots, M_{\text{pts}} - 1$.

Using (9), the temporal estimate within this approximation window can be represented as

$$\begin{aligned} & \hat{H}[a \cdot I_p, b \cdot K_p] \\ &= \sum_{i=0}^{I_{\text{deg}}} \sum_{j=0}^{J_{\text{deg}}} C_{n_0, k_0}[i, j] (a \cdot I_p - n_0)^i (b \cdot K_p - k_0)^j \\ &+ S'_{I_{\text{deg}} J_{\text{deg}}}[a \cdot I_p, b \cdot K_p] \quad \text{for } a = 0, 1, \dots, L_{\text{pts}} - 1 \text{ and } b = 0, 1, \dots, M_{\text{pts}} - 1 \quad (10) \end{aligned}$$

where $(n_0, k_0) = (L, M)$ is the center of the approximation window. Since the temporal estimates $\hat{H}[a \cdot I_p, b \cdot K_p]$ are noisy samples of the true channel frequency response, the residue term $S'_{I_{\text{deg}} J_{\text{deg}}}[a \cdot I_p, b \cdot K_p]$ includes the model error as well as the noise. In order to determine $(I_{\text{deg}} + 1) \times (J_{\text{deg}} + 1)$ unknown

polynomial coefficients from the temporal estimation, it is necessary to have at least $(I_{\text{deg}} + 1) \times (J_{\text{deg}} + 1)$ equations in (10). That is, $L_{\text{pts}} \geq I_{\text{deg}} + 1$, and $M_{\text{pts}} \geq J_{\text{deg}} + 1$.

Equation (10) can also be written in matrix format. Let $[A]_{i,j}$ denote the element on the i th row and the j th column of matrix A . We define the following matrices as

$$\begin{aligned} & \check{\mathbf{H}}_{n_0, k_0} \text{ with size } L_{\text{pts}} \times M_{\text{pts}}, \quad \text{and} \\ & [\check{\mathbf{H}}_{n_0, k_0}]_{i,j} = \hat{H}[i \cdot I_p, j \cdot K_p] \\ & \mathbf{q}_{I_{\text{deg}}} \text{ with size } L_{\text{pts}} \times (I_{\text{deg}} + 1), \quad \text{and} \\ & [\mathbf{q}_{I_{\text{deg}}}]_{i,j} = (i \cdot I_p - n_0)^j \\ & \mathbf{C}_{I_{\text{deg}} J_{\text{deg}}} \text{ with size } (I_{\text{deg}} + 1) \times (J_{\text{deg}} + 1), \quad \text{and} \\ & [\mathbf{C}_{I_{\text{deg}} J_{\text{deg}}}]_{i,j} = C_{n_0, k_0}[i, j] \\ & \mathbf{q}_{J_{\text{deg}}} \text{ with size } M_{\text{pts}} \times (J_{\text{deg}} + 1), \quad \text{and} \\ & [\mathbf{q}_{J_{\text{deg}}}]_{i,j} = (i \cdot K_p - k_0)^j \\ & \mathbf{S}'_{I_{\text{deg}} J_{\text{deg}}} \text{ with size } L_{\text{pts}} \times M_{\text{pts}}, \quad \text{and} \\ & [\mathbf{S}'_{I_{\text{deg}} J_{\text{deg}}}]_{i,j} = S'_{I_{\text{deg}} J_{\text{deg}}}[i \cdot I_p, j \cdot K_p]. \end{aligned}$$

We can show that (10) is equivalent to

$$\check{\mathbf{H}}_{n_0, k_0} = \mathbf{q}_{I_{\text{deg}}} \mathbf{C}_{I_{\text{deg}} J_{\text{deg}}} \mathbf{q}_{J_{\text{deg}}}^T + \mathbf{S}'_{I_{\text{deg}} J_{\text{deg}}}. \quad (11)$$

Let $\text{vec}(\mathbf{A})$ denote the vector whose elements are taken column-wise from matrix \mathbf{A} , and let \otimes denote the Kronecker product. The Kronecker product has the following property [26]:

$$\mathbf{Y} = \mathbf{B} \mathbf{X} \mathbf{A}^T \Leftrightarrow \text{vec}(\mathbf{Y}) = (\mathbf{A} \otimes \mathbf{B}) \text{vec}(\mathbf{X}). \quad (12)$$

Using this property, (11) can be written as

$$\check{\mathbf{h}}_{n_0, k_0} = (\mathbf{q}_{J_{\text{deg}}} \otimes \mathbf{q}_{I_{\text{deg}}}) \mathbf{c}_{I_{\text{deg}} J_{\text{deg}}} + \mathbf{s}'_{I_{\text{deg}} J_{\text{deg}}} \quad (13)$$

where $\check{\mathbf{h}}_{n_0, k_0} = \text{vec}(\check{\mathbf{H}}_{n_0, k_0})$, $\mathbf{c}_{I_{\text{deg}} J_{\text{deg}}} = \text{vec}(\mathbf{C}_{I_{\text{deg}} J_{\text{deg}}})$, and $\mathbf{s}'_{I_{\text{deg}} J_{\text{deg}}} = \text{vec}(\mathbf{S}'_{I_{\text{deg}} J_{\text{deg}}})$.

In (13), $\check{\mathbf{h}}_{n_0, k_0}$ contains the temporal estimates of the channel parameters that are obtained from training pilots using (8), $\mathbf{c}_{I_{\text{deg}} J_{\text{deg}}}$ contains the polynomial coefficients to be estimated, and $\mathbf{s}'_{I_{\text{deg}} J_{\text{deg}}}$ is the error term. Therefore, the least square solution of the polynomial coefficients, which is denoted by $\hat{\mathbf{c}}_{I_{\text{deg}} J_{\text{deg}}}$, is calculated as

$$\hat{\mathbf{c}}_{I_{\text{deg}} J_{\text{deg}}} = (\mathbf{q}_{J_{\text{deg}}} \otimes \mathbf{q}_{I_{\text{deg}}})^\dagger \check{\mathbf{h}}_{n_0, k_0} \quad (14)$$

where \mathbf{A}^\dagger denotes the pseudo-inverse of matrix \mathbf{A} .

The next step is to compute the channel frequency response of all subchannels from the estimated polynomial coefficients. In the approximation window, the estimated channel parameters are represented by a $(2L+1) \times (2M+1)$ matrix $\hat{\mathbf{H}}_{n_0, k_0}$, and $[\hat{\mathbf{H}}_{n_0, k_0}]_{i,j} = \hat{H}[i, j]$. In addition, we denote $\hat{\mathbf{h}}_{n_0, k_0} = \text{vec}(\hat{\mathbf{H}}_{n_0, k_0})$ and define matrices

$$\begin{aligned} & \mathbf{Q}_{I_{\text{deg}}} \text{ with size } (2L+1) \times (I_{\text{deg}} + 1), \quad \text{and} \\ & [\mathbf{Q}_{I_{\text{deg}}}]_{i,j} = (i - L)^j \\ & \mathbf{Q}_{J_{\text{deg}}} \text{ with size } (2M+1) \times (J_{\text{deg}} + 1), \quad \text{and} \\ & [\mathbf{Q}_{J_{\text{deg}}}]_{i,j} = (i - M)^j. \end{aligned}$$

Then, the channel responses in the approximation window are estimated as

$$\hat{\mathbf{h}}_{n_0, k_0} = (\mathbf{Q}_{J_{\text{deg}}} \otimes \mathbf{Q}_{I_{\text{deg}}}) \hat{\mathbf{c}}_{I_{\text{deg}} J_{\text{deg}}} \quad (15)$$

$$= (\mathbf{Q}_{J_{\text{deg}}} \otimes \mathbf{Q}_{I_{\text{deg}}}) (\mathbf{q}_{J_{\text{deg}}} \otimes \mathbf{q}_{I_{\text{deg}}})^\dagger \check{\mathbf{h}}_{n_0, k_0} \quad (16)$$

$$= (\mathbf{Q}_{J_{\text{deg}}} \mathbf{q}_{J_{\text{deg}}}^\dagger \otimes \mathbf{Q}_{I_{\text{deg}}} \mathbf{q}_{I_{\text{deg}}}^\dagger) \check{\mathbf{h}}_{n_0, k_0}. \quad (17)$$

Here, (15) is based on (9), (16) is derived from (14) and (15), and (17) is obtained using the properties of Kronecker product $(A \otimes B)(C \otimes D) = (AC \otimes BD)$ and $(A \otimes B)^\dagger = (A^\dagger \otimes B^\dagger)$ [26].

Using (12) and (17), we can show that

$$\hat{\mathbf{H}}_{n_0, k_0} = (\mathbf{Q}_{I_{\text{deg}}} \mathbf{q}_{I_{\text{deg}}}^\dagger) \check{\mathbf{H}}_{n_0, k_0} (\mathbf{Q}_{J_{\text{deg}}} \mathbf{q}_{J_{\text{deg}}}^\dagger)^T. \quad (18)$$

From an implementation point of view, the terms $(\mathbf{Q}_{I_{\text{deg}}} \mathbf{q}_{I_{\text{deg}}}^\dagger)$ and $(\mathbf{Q}_{J_{\text{deg}}} \mathbf{q}_{J_{\text{deg}}}^\dagger)$ can be computed off-line. Thus, the channel responses in one approximation window can be obtained from the temporal estimation by i) a multiplication of a $(2L+1) \times L_{\text{pts}}$ matrix and an $L_{\text{pts}} \times M_{\text{pts}}$ matrix and ii) a multiplication of a $(2L+1) \times M_{\text{pts}}$ matrix and an $M_{\text{pts}} \times (2M+1)$ matrix. Based on the above discussion, the polynomial-based PSA channel estimation can be performed using the following procedures.

Off-line Computation:

- 1) Determine the degrees of polynomial basis functions $(I_{\text{deg}}, J_{\text{deg}})$ and the window size (L, M) based on the training pattern and the channel conditions.
- 2) Calculate $(\mathbf{Q}_{I_{\text{deg}}} \mathbf{q}_{I_{\text{deg}}}^\dagger)$ and $(\mathbf{Q}_{J_{\text{deg}}} \mathbf{q}_{J_{\text{deg}}}^\dagger)$.

On-line Computation:

- 1) Compute the temporal estimation in $(2M+1)$ consecutive OFDM blocks.
- 2) Slide the approximation windows over these total $N \times (2M+1)$ subchannels, such that all subchannels are covered by at least one window. Then, compute the channel parameters in each window from the temporal estimation based on (18). Note that the matrix indexes should be adjusted according to the window centers when using (18).

The parameters in polynomial-based PSA channel estimation, including pilot spacing, polynomial degree, and window size, should be chosen to minimize the channel estimation error for given channel conditions. Unfortunately, there is no closed-form solution for such an optimization problem. In [15], the optimal parameters for decision-directed methods were obtained using exhaustive search for a given channel correlation function. In this paper, we choose the parameters as $L_{\text{pts}} = I_{\text{deg}} + 1$, $M_{\text{pts}} = J_{\text{deg}} + 1$, and $I_{\text{deg}} = J_{\text{deg}} = 3$. Thus, the approximation window size only depends on the pilot spacing, as $(I_{\text{deg}} I_p + 1) \times (J_{\text{deg}} K_p + 1)$. We obtain these parameters by performing simulations over a broad range of channel conditions, and they demonstrate good performance in most channels. In particular, we performed simulation for Typical Urban (TU) and Hilly Terrain (HT) delay profiles [19], [27] for Doppler frequency from 40 to 200 Hz and for channel SNR from 5 dB to 40 dB. Here, Both of the delay

profiles have six paths. The average path power and delay for the TU delay profile are $\sigma_i^2 = \{0.5, 1.0, 0.63, 0.26, 0.16, 0.1\}$, and $\tau_i = \{0, 0.2 \mu\text{s}, 0.5 \mu\text{s}, 1.6 \mu\text{s}, 2.3 \mu\text{s}, \text{ and } 5.0 \mu\text{s}\}$, and the average path power and delay for the HT delay profile are $\sigma_i^2 = \{1.0, 0.64, 0.4, 0.2, 0.26, 0.06\}$ and $\tau_i = \{0, 0.2 \mu\text{s}, 0.4 \mu\text{s}, 0.6 \mu\text{s}, 15.0 \mu\text{s}, 17.2 \mu\text{s}\}$.

B. Channel Estimation Error and Decoding BER

Instead of finding the channel estimation error averaged over all subchannels, we are more interested in calculating the channel estimation error of individual subchannel. Let $\varepsilon_{\text{MSE}}^2[n, k]$ denote the mean square channel estimation error of the n th subchannel in the k th OFDM block, i.e., $\varepsilon_{\text{MSE}}^2[n, k] = E[(H[n, k] - \hat{H}[n, k])(H[n, k] - \hat{H}[n, k])^*]$. Then, the MSE channel estimation of all subchannels in one estimation window can be described by a $(2L+1)(2M+1) \times 1$ vector as

$$\varepsilon_{\text{MSE}}^2 \equiv [\varepsilon_{\text{MSE}}^2[0, 0], \dots, \varepsilon_{\text{MSE}}^2[2L, 0], \varepsilon_{\text{MSE}}^2[0, 1], \dots, \varepsilon_{\text{MSE}}^2[2L, 1], \dots, \varepsilon_{\text{MSE}}^2[2L, 2M]]^T. \quad (19)$$

Similar to Section III-A, matrices \mathbf{H}_{n_0, k_0} and $\hat{\mathbf{H}}_{n_0, k_0}$ represent the true and estimated channel responses in one approximation window, respectively. Both matrices have size $(2L+1) \times (2M+1)$. For the window centered at (n_0, k_0) , $[\mathbf{H}_{n_0, k_0}]_{i, j} = H[i - L + n_0, j - M + k_0]$, and $[\hat{\mathbf{H}}_{n_0, k_0}]_{i, j} = \hat{H}[i - L + n_0, j - M + k_0]$. The vector representations of these two matrices are $\mathbf{h}_{n_0, k_0} = \text{vec}(\mathbf{H}_{n_0, k_0})$ and $\hat{\mathbf{h}}_{n_0, k_0} = \text{vec}(\hat{\mathbf{H}}_{n_0, k_0})$. Thus, (19) is equivalent to

$$\varepsilon_{\text{MSE}}^2 = \text{diag} \left(E \left[\left(\mathbf{h}_{n_0, k_0} - \hat{\mathbf{h}}_{n_0, k_0} \right) \times \left(\mathbf{h}_{n_0, k_0} - \hat{\mathbf{h}}_{n_0, k_0} \right)^H \right] \right). \quad (20)$$

From (16) and (20), we obtain

$$\varepsilon_{\text{MSE}}^2 = \text{diag} \left\{ \left(E \left[\left(\mathbf{h}_{n_0, k_0} - (\mathbf{Q}_{J_{\text{deg}}} \otimes \mathbf{Q}_{I_{\text{deg}}}) \times (\mathbf{q}_{J_{\text{deg}}} \otimes \mathbf{q}_{I_{\text{deg}}})^\dagger \check{\mathbf{h}}_{n_0, k_0} \right) \times \left(\mathbf{h}_{n_0, k_0} - (\mathbf{Q}_{J_{\text{deg}}} \otimes \mathbf{Q}_{I_{\text{deg}}}) \times (\mathbf{q}_{J_{\text{deg}}} \otimes \mathbf{q}_{I_{\text{deg}}})^\dagger \check{\mathbf{h}}_{n_0, k_0} \right)^H \right] \right) \right\}. \quad (21)$$

Using the channel delay profile, Doppler frequency, and channel SNR, the channel estimation error can be calculated.

For M-QAM modulation, the effect of channel estimation on the BER has been discussed in [28] and [29]. Particularly, [29] gave the close form expression of the BER in OFDM systems with imperfect channel estimation. Using the results in [29] and (21), we calculate the BER of different OFDM subchannels. Fig. 3(a) shows the mean square channel estimation error calculated from (21) for the typical urban (TU) delay profile [19], [27] with Doppler frequency 200 Hz and channel SNR 30 dB. The pilot spacing $I_p = K_p = 4$ is used. This implies that the

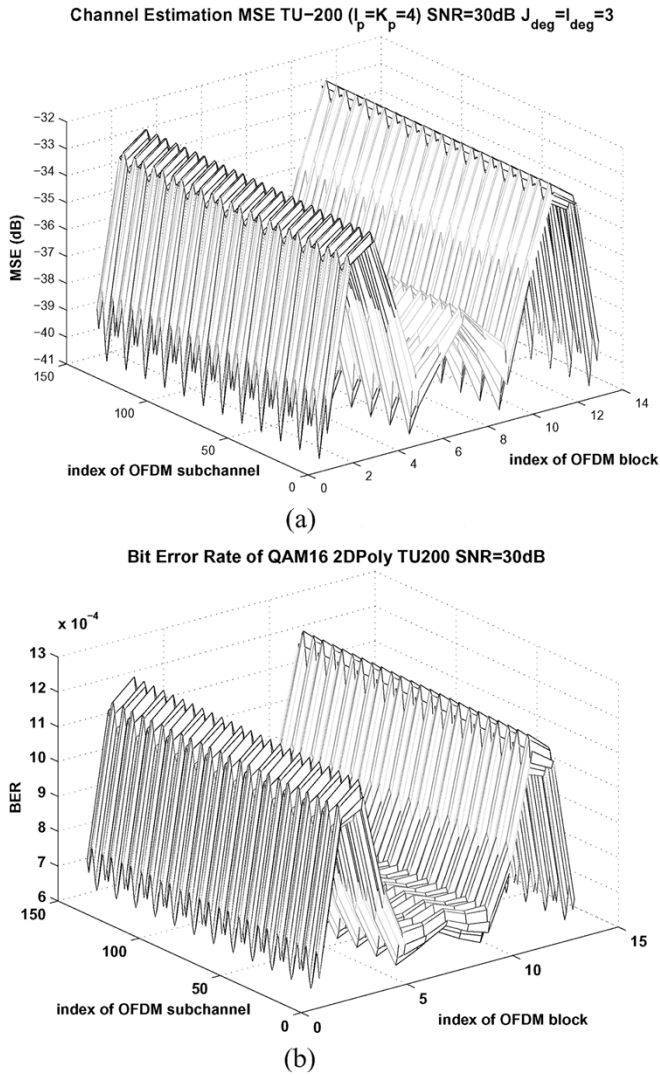


Fig. 3. Channel estimation MSE and decoding BER when using polynomial-based channel estimation. (a) Channel estimation MSE, TU-200, SNR = 30 dB. (b) BER, TU-200, SNR = 30 dB, QAM16.

approximation window size is 13 by 13, as discussed in Section III-A. From Fig. 3(a), we can see that the channel estimation error varies significantly for different subchannels and OFDM blocks. In addition, the corresponding BER for using 16-QAM modulation is shown in Fig. 3(b). It is clear that the subchannels that have larger channel estimation error experience higher decoding BER.

C. Priority Transmission Design for 2-D Polynomial Channel Estimation

In the previous section, we have seen that there exists significant BER variation across different OFDM subchannels due to channel estimation inaccuracy. For multimedia data transmission, we can utilize this property to provide unequal error protection (UEP). In this section, we design the priority transmission (PT) scheme, which rearranges multimedia data in OFDM subchannels by jointly considering the effects of channel estimation and the importance of multimedia data. In particular, the PT scheme is applied in the following four steps.

- Step 1) Calculate mean square channel estimation error in one approximation window, based on channel estimation parameters ($I_p, K_p, I_{deg}, J_{deg}, M_{pts}, N_{pts}$) and the channel correlation matrix. Here, the channel correlation can be obtained through feedback from the receivers.
- Step 2) Sort all subchannels within $D \times K_p \times J_{deg}$ OFDM blocks in the increasing order of BER. Here, D is the PT delay parameter and should be determined such that the maximum decoding delay allowed at the receiver is less than the time used to transmit $D \times K_p \times J_{deg}$ consecutive OFDM blocks.
- Step 3) Rearrange the encoded multimedia bitstream in the decreasing order of importance.
- Step 4) Match the rearranged multimedia data with the sorted subchannels such that higher importance of the multimedia data are transmitted over the subchannels with lower BER.

The total decoding delay at the receiver depends on the parameter D as well as the approximation window size. Since the receiver must receive all the pilot symbols in one approximation window before performing channel estimation, the decoding delay caused by channel estimation is $K_p \times J_{deg}$ OFDM blocks. By applying PT, the receiver must obtain $D \times K_p \times J_{deg}$ consecutive OFDM blocks before rearranging the received data back into their original order. Thus, the decoding delay of the OFDM system with polynomial-based PSA channel estimation and PT is $D \times K_p \times J_{deg}$ OFDM blocks. We note that the performance of the PT depends on the delay parameters D . When larger delay parameter D is allowed, the PT scheme will have more flexibility in arranging the transmission order of data and will achieve better quality in reconstructed multimedia.

For multimedia transmission, UEP can also be achieved by applying forward error correction (FEC) codes with different rates to different portions of multimedia data stream. Compared to FEC-based UEP methods, such as those in [23] and [24], the PT scheme has the advantage of not introducing additional redundancy. Furthermore, the PT scheme can work together with FEC-based methods when both the BER variation of channel estimation and the importance of multimedia data are taken into consideration for choosing the channel coding rates.

D. PT Scheme Based on Polynomial Channel Estimation: Simulation Results

We simulate image transmission in an OFDM system with the following parameters to demonstrate the performance of the PT scheme. The transmitted data is a 512 by 512 Lena image, which is compressed to 0.5 bit/pixel using SPIHT [13]. The compressed bitstream is packetized into 128 bit long packets. Each packet is appended with a 16-bit CRC code [30], [31] and then encoded using the shortened systematic RS(30, 18) code, which is obtained by shortening RS(255 225) in GF(2^8) [2]. The encoded data are transmitted in an OFDM system, where the entire channel bandwidth is 800 kHz, with 128 subchannels. In each OFDM block, four boundary subchannels at each end are used as guard tones [10], and the remaining 120 subchannels are used to transmit data. To eliminate ISI, a 32 symbol

long cyclic prefix is inserted in each OFDM block [7]. All subchannels use QAM16 modulation. Rectangular pilot configuration with $I_p = K_p = 4$ is used in the TU delay profile, and $I_p = 2, K_p = 4$ is used in the HT delay profile. At the receiver, error check is performed based on the CRC-16 code after RS decoding. If there are irrecoverable errors in a packet, this packet is dropped. The first dropped packet stops the SPIHT decoder. We employ the peak-signal-to-noise ratio (PSNR) of the reconstructed image as our performance measure. The PSNR is defined as

$$\text{PSNR} = 10 \log_{10} \left(\frac{255^2}{\text{MSE}} \right) \text{ dB} \quad (22)$$

where MSE denotes the mean-square-error of the reconstructed image.

Three transmission strategies are compared. The first scheme, which is referred to as the *Interleaving 1*, transmits the encoded bitstream according to the following order: $\{(n, k) = (0, 0), (0, K_p \times J_{\text{deg}}), \dots, (0, (D - 1) \times K_p \times J_{\text{deg}}), (1, 0), (1, K_p \times J_{\text{deg}}), \dots, (1, (D - 1) \times K_p \times J_{\text{deg}}), \dots, (N - 1, 0), (N - 1, K_p \times J_{\text{deg}}), \dots, (N - 1, (D - 1) \times K_p \times J_{\text{deg}}), (0, 1), (0, K_p \times J_{\text{deg}} + 1), \dots, (0, (D - 1) \times K_p \times J_{\text{deg}} + 1), (1, 1), \dots\}$, where n is the index of OFDM subchannels, and k denotes the index of OFDM blocks. We note that when $D = 1$, the *Interleaving 1* becomes the regular transmission that transmits the encoded image block by block according to the order $\{(n, k) = (0, 0), (1, 0), \dots, (N - 1, 0), (0, 1), \dots, (N - 1, 1), \dots\}$. The second scheme, which is referred to as the *Interleaving 2*, transmits data according to the order $\{(n, k) = (0, 0), (0, K_p \times J_{\text{deg}}), \dots, (0, (D - 1) \times K_p \times J_{\text{deg}}), (0, 1), (0, K_p \times J_{\text{deg}} + 1), \dots, (0, (D - 1) \times K_p \times J_{\text{deg}} + 1), \dots, (0, D \times K_p \times J_{\text{deg}} - 1), (1, 0), (1, K_p \times J_{\text{deg}}), \dots, (1, (D - 1) \times K_p \times J_{\text{deg}}), \dots\}$. When $D = 1$, the *Interleaving 2* scheme transmits according to order $\{(n, k) = (0, 0), (0, 1), \dots, (0, K_p \times J_{\text{deg}} - 1), (1, 0), \dots, (1, K_p \times J_{\text{deg}} - 1), \dots, (N - 1, 1), \dots, (N - 1, K_p \times J_{\text{deg}} - 1)\}$. The third scheme is the PT scheme, which rearranges the transmission order of the multimedia data within $D \times K_p \times J_{\text{deg}}$ OFDM blocks according to channel estimation errors. In the simulations, we assume the perfect estimation of channel correlation matrix (Step 1) in the PT scheme.

Fig. 4 shows the average PSNR of reconstructed images in three transmission schemes. Fig. 4(a) and (b) are for the TU and HT delay profiles, respectively, with the maximum Doppler frequency 200 Hz. The results are obtained by averaging 300 transmissions of Lena image for different fading and additive noise realizations. One can observe that the PT scheme performs better or at least as well as the regular transmission (*Interleave 1*, $D = 1$) and *Interleave 2* with $D = 1$. Moreover, the performance gain of the PT scheme is larger when the delay parameter D is larger. This is due to the fact that there are effectively larger number of good OFDM subchannels to transmit the more important SPIHT bitstreams when the delay parameter D is larger. Compared with the *Interleave 1* and *Interleave 2* schemes, the PT scheme achieves about a 4- and 8-dB gain in reconstructed PSNR when the delay parameter $D = 24$ and the channel SNR is equal to 21 dB in TU delay profile with 200-Hz doppler frequency. With the same delay parameter D , all the three transmis-

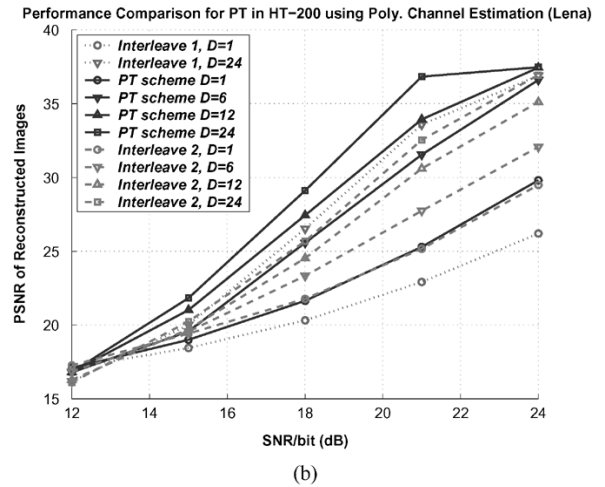
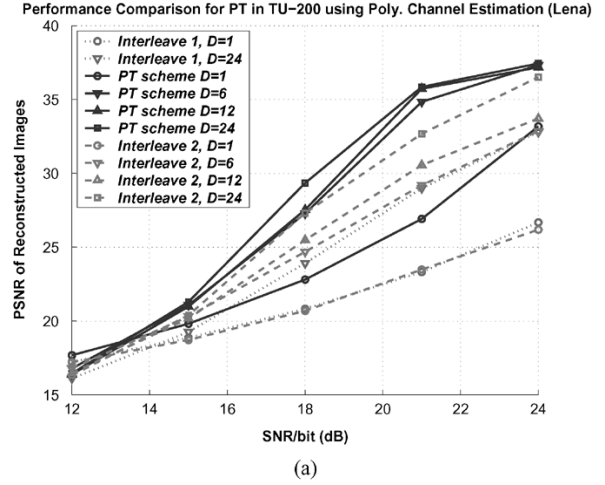


Fig. 4. Comparison of the three transmission schemes using polynomial-based channel estimation. (a) TU delay profile ($f_D = 200$ Hz, $I_p = K_p = 4$). (b) HT delay profile ($f_D = 200$ Hz, $I_p = 2, K_p = 4$).

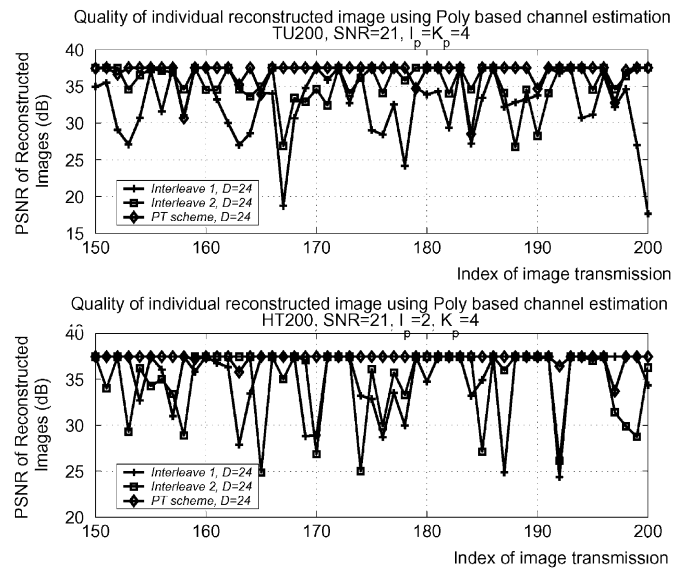


Fig. 5. PSNR of individual reconstructed images of the three transmission schemes using polynomial channel estimation.

sion schemes have similar interleaving benefit. Thus, the gain of the PT scheme is mainly from allocating the more impor-

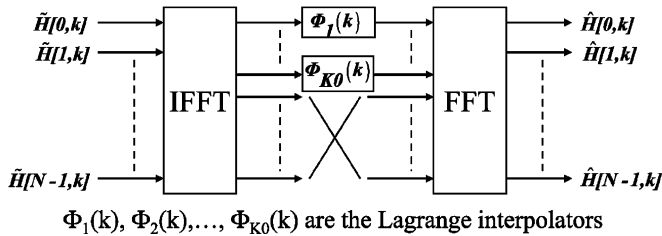


Fig. 6. FFT-based channel estimation scheme.

tant data to subchannels experiencing lower channel estimation error. Fig. 5 shows the PSNR of individual reconstructed images. Here, the Doppler frequency is 200 Hz, and both TU and HT delay profiles are studied. When using the PT, the PSNR of the reconstructed images at different time instances does not change much, whereas two other transmission schemes do not have this advantage. Obviously, the PT scheme provides better and smoother performance over time.

IV. PRIORITY TRANSMISSION BASED ON FFT-BASED CHANNEL ESTIMATION

The FFT-based channel estimation has been well studied for both the decision-directed [7], [8] and PSA scenarios [9], [10], [17], [22]. In this section, we design the PT scheme for the FFT-based PSA channel estimation. As discussed in Section III, the crucial idea behind the PT scheme is to evaluate the error performance of individual OFDM subchannels and to load multimedia data according to the quality of the subchannels. Thus, we first briefly summarize the FFT-based channel estimation algorithm and design the PT scheme to improve the reliability of multimedia transmission.

A. FFT-Based Channel Estimation: Algorithm Description

The structure of FFT-based channel estimation in [7] and [9] is illustrated in Fig. 6. The input $\hat{H}(n, k)$ is obtained from the temporal estimation as

$$\hat{H}(n, k) = \begin{cases} Y[n, k]/X[n, k], & \text{when } (n, k) \text{ are pilot positions} \\ 0, & \text{otherwise.} \end{cases}$$

The first K_0 outputs of the IFFT, representing low-frequency components, are interpolated by the interpolation filters, which are denoted by $\phi_1, \phi_2, \dots, \phi_{K_0}$. Here, K_0 is computed as $K_0 = (\lfloor B_d \times \tau_{\max} \rfloor + 1)$ [7], where B_d is the total channel bandwidth, and τ_{\max} is the maximum delay spread. In [9], the Lagrange interpolators are chosen. The rest of the high-frequency components after IFFT are set to zeros. The estimated channel parameters, which are denoted by $\hat{H}(n, k)$, are obtained after the FFT operation. In this channel estimation scheme, the frequency domain interpolation is performed through IFFT-FFT filtering, whereas the time domain interpolation is performed by the Lagrange interpolators. Consequently, the channel responses for all subchannels are estimated.

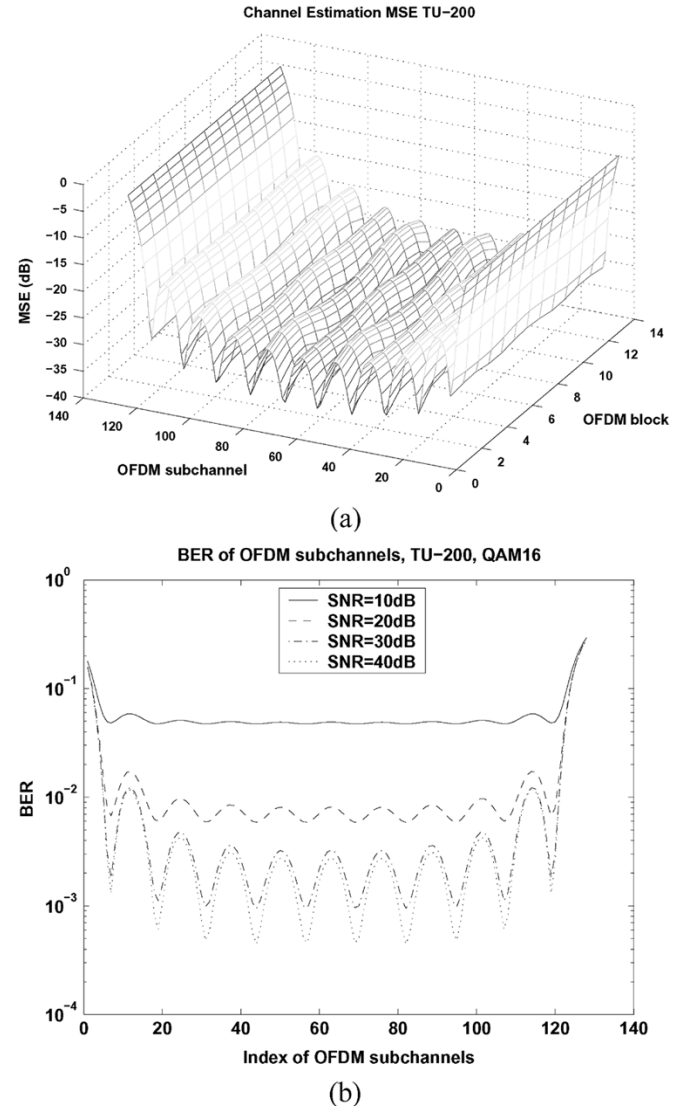


Fig. 7. Channel estimation MSE and decoding BER when using FFT-based channel estimation. (a) MSE TU-200, SNR = 30 dB, QAM16. (b) BER TU-200, SNR = 30 dB, QAM16.

B. FFT-Based Channel Estimation: Channel Estimation Error and BER

FFT-based PSA channel estimation can be applied on a variety of pilot patterns. For the purpose of fair comparison between FFT-based and polynomial-based methods in later sections, we demonstrate the performance of the FFT-based methods using the rectangular training pattern. Without loss of generality, we consider the channel estimation in $(L_{\text{deg}}K_p + 1)$ consecutive OFDM blocks, which have indexes $\{k, k = 0, \dots, L_{\text{deg}}K_p\}$. Here, L_{deg} is the degree of the Lagrange interpolation.

Given the channel correlation functions [as in (5)–(7)], the channel estimation MSE can be calculated in a similar way as that in Section III-B, which is omitted in this paper. Fig. 7(a) shows the channel estimation mean square error for the TU delay profile with Doppler frequency 200 Hz and channel SNR 30 dB. The pilot spacing is chosen as $I_p = K_p = 4$, and L_{deg} is chosen to be 3. We observe that there exists a significant

variation in channel estimation errors along different OFDM subchannels, which is often referred to as the *leakage effect* [6]–[8], [17]. The leakage effect occurs when the delay paths τ_i are not all integer multiples of the system sampling period [6], [7], [17]. Since it is not realistic for all delay paths to be exactly integer multiples of the sampling period, the leakage effect always causes performance degradation in FFT-based channel estimation. In Fig. 7(b), the decoding BER of subchannels in one OFDM block calculated from the estimation MSE using the results in [29] is shown for different channel SNR in the TU delay profile with Doppler frequency 200 Hz. One can see that the leakage effect will not diminish, even when channel SNR is high. Compared to the error variation in the polynomial-based methods (see Fig. 3), the error variation in the FFT-based methods is larger. This leakage effect is difficult to eliminate and is typically remedied by discarding a large number of boundary subchannels [17] or performing adaptive bit/power loading [32] that requires high computational complexity. In this work, we utilize this property to provide unequal error protection (UEP) for multimedia transmission.

C. Priority Transmission Design for FFT-Based Channel Estimator

Similar to Section III, the priority transmission utilizes the variation of BER and provides UEP for multimedia data. The procedure of the PT is the same as that in Section III-C with some slight modifications in the first step. In the first step of the PT with the FFT-based channel estimation, the channel estimation MSE is calculated based on pilot spacing, Doppler frequency, maximum path delay, total bandwidth, and degree of Lagrange interpolation. The decoding delay introduced by the FFT-based channel estimation is $(L_{\text{deg}}K_p + 1)$ OFDM blocks, and that of the PT is $D \times L_{\text{deg}} \times K_p$ OFDM blocks. Thus, the total decoding delay is $D \times L_{\text{deg}} \times K_p$. The parameter D can be adjusted to provide the tradeoff between the decoding delay and the quality of reconstructed multimedia.

D. PT Scheme Based on FFT-Based Channel Estimation: Simulation Results

In this section, we evaluate the effectiveness of the PT for FFT-based channel estimation through simulations. The performance of the PT in both FFT-based and polynomial-based methods will be compared in Section V. Similar to Section III-D, three transmission schemes will be compared. They are the *Interleave 1*, *Interleave 2*, and PT scheme. All other simulation parameters are the same as those in Section III-D. Fig. 8 shows the simulation results for various decoding delay and channel SNR. Fig. 8(a) is for the TU delay profile, and Fig. 8(b) is for the HT delay profile. Compared with the methods that do not utilize the channel estimation property, the PT scheme can significantly improve the PSNR of the reconstructed images in moderate and high channel SNR regions, where most practical wireless systems operate. For example, the PT scheme outperforms the *Interleave 1* and *Interleave 2* with $D = 1$ in TU-200 by 1 and 2 dB in PSNR of the reconstructed image when channel SNR equals to 21 dB. The performance gain of the PT scheme is more pronounced when the delay parameter D is larger. That is, the PT scheme achieves 11 and 9 dB higher in the PSNR

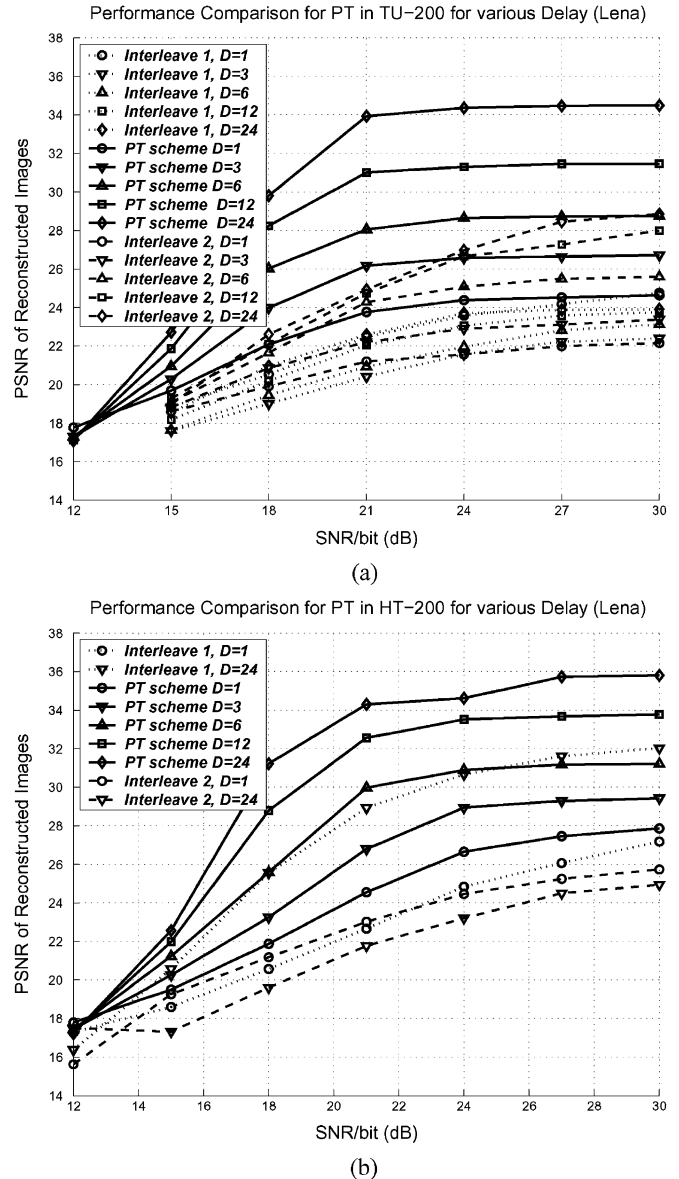


Fig. 8. Comparison between the three transmission schemes for various wireless channel conditions and decoding delay. (a) TU delay profile $f_D = 200$ Hz. (b) HT delay profile $f_D = 200$ Hz.

of the reconstructed image when it is compared with *Interleave 1* and *Interleave 2* with $D = 24$, and channel SNR equals 21 dB. The reason for this higher performance gain is that the PT scheme effectively has larger number of good subchannels to transmit more important multimedia data. The PSNR of individual reconstructed images are shown in Fig. 9 for the *Interleave 1*, *Interleave 2*, and PT scheme for $D = 24$. When using the *Interleave 1* and *Interleave 2* schemes, the quality of the subchannels that transmits the more important bits of the SPIHT bitstream is quite random. Thus, the quality of individual received images changes rapidly. When using the PT, the data is allocated according to the importance of data and the quality of the subchannels. In this case, the transmission of each image experiences similar channel conditions, and smooth quality of the reconstructed images is achieved.

We also simulate the case when using the *shifted-pilot* configuration, that is, the pilots are placed on subchannels

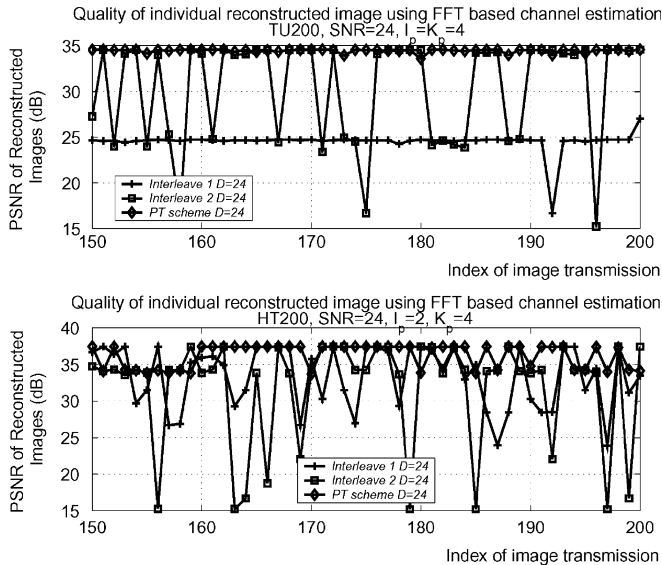


Fig. 9. PSNR of individual reconstructed images of three transmission schemes.

$0, I_p, 2I_p, \dots$, in the 0 th OFDM block, and they are placed on subchannels $1, I_p + 1, 2I_p + 1, \dots$, in the K_p th OFDM block. We note that this shifted pilot has been used in several practical transmission standards such as DAB [1] and DVB [2]. The performance of the PT scheme is shown in Fig. 10. Similar to the rectangular pilot case, the PT scheme always achieves higher performance compared with the schemes that do not utilize the channel estimation error property. We note that the calculation of channel estimation MSE and subchannel reordering in PT for the shifted pilot takes the pilot pattern into consideration. Within the acceptable delay, the PT scheme tries to match the characteristic of multimedia to the OFDM channel by allocating the more important multimedia data onto the better subchannels.

Comparing Figs. 8(a) and 10(a) [correspondingly Figs. 8(b) and 10(b)], we observe that the performance of the PT scheme in the shifted pilot is slightly better or almost the same as the one without shifted pilot. For the Interleave 1 and 2 schemes, their performances are comparable when the delay parameter is one; however, they become worse when the Delay parameter is large. This can be explained as follows. The interleave 1 and 2 schemes with delay parameter virtually fill the near boundary OFDM subchannel with the more important data while expecting some interleaving benefit. When using with the shifted pilot, both of the schemes are more likely to use bad subchannels near the OFDM block boundaries. Therefore, the resulting performances are worse than the ones without shifted pilot. This effect can be compensated by discarding more boundary subchannels, as demonstrated below. We simulate the same condition for TU-200 case, except that eight boundary subchannels at each end of one OFDM block are used as guard tone, and the remaining 112 subchannels are used for transmitting the multimedia data. The resulting performance comparisons are shown in Fig. 11. It is clear from the figure that interleaving schemes with delay perform better than without delay case. However, the larger the number of subchannels are discarded, the more

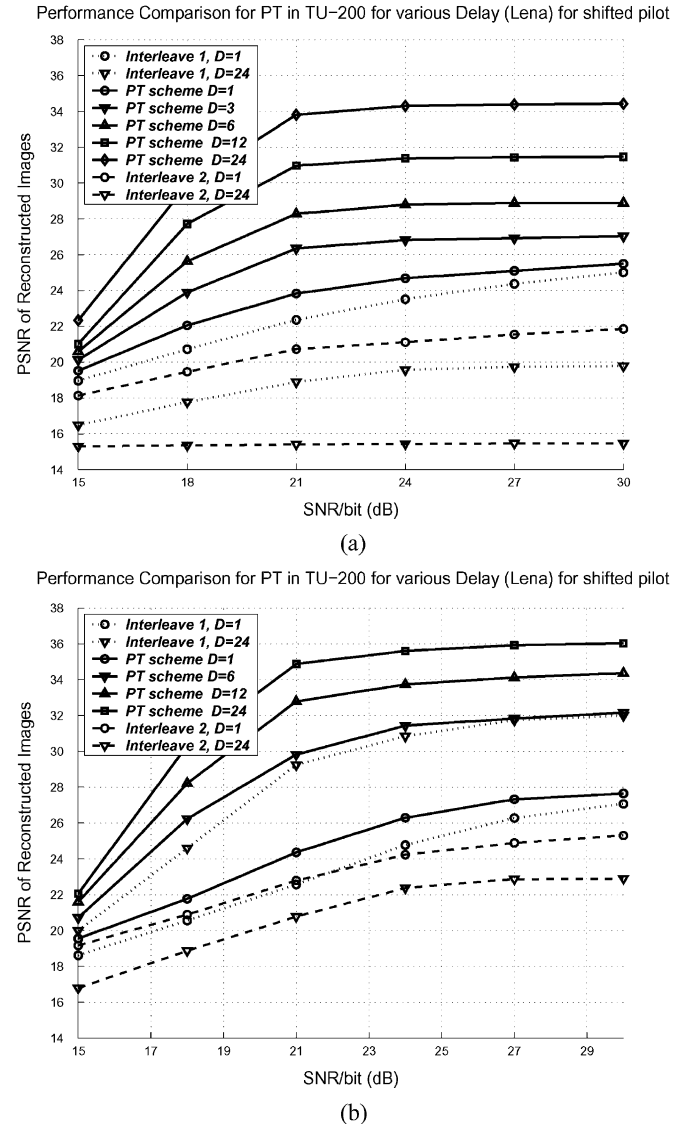


Fig. 10. Comparison between the three transmission schemes for shifted pilot pattern in various wireless channel conditions and decoding delay. (a) TU delay profile $f_D = 200$ Hz. (b) HT delay profile $f_D = 200$ Hz.

OFDM blocks should be used for transmitting an image. Similar to the previous scenario, the PT scheme in this case also performs much better compared with the one where the guard tone is four. This is because the worse channels have been discarded. In all simulations, the PT scheme provides significant gain over the one that does not exploit the channel estimation property.

V. COMPARISON BETWEEN FFT-BASED METHOD AND POLYNOMIAL-BASED METHOD

The FFT- and polynomial-based channel estimation methods have been compared for data transmission in decision-directed scenario [15], [16]. Since we have developed the polynomial-based PSA channel estimation, we can compare the FFT- and polynomial-based channel estimation in the PSA scenario. In this section, we will first compare these two types of PSA channel estimation techniques for generic data transmission

Performance Comparison for PT in TU-200 for various Delay (Lena) for shifted pilot

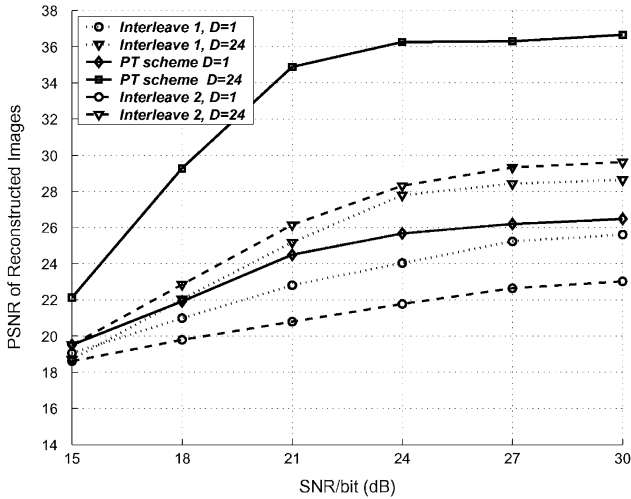


Fig. 11. TU delay profile $f_D = 200$ Hz, guard tone = 8.

by examining their average BER performances for different channel SNR and training pilot density. More importantly, since the OFDM modulation is adopted in many broadband multimedia transmission standards, such as DVB-T, it is particularly interesting to perform the comparison for multimedia transmission when the proposed PT schemes are employed.

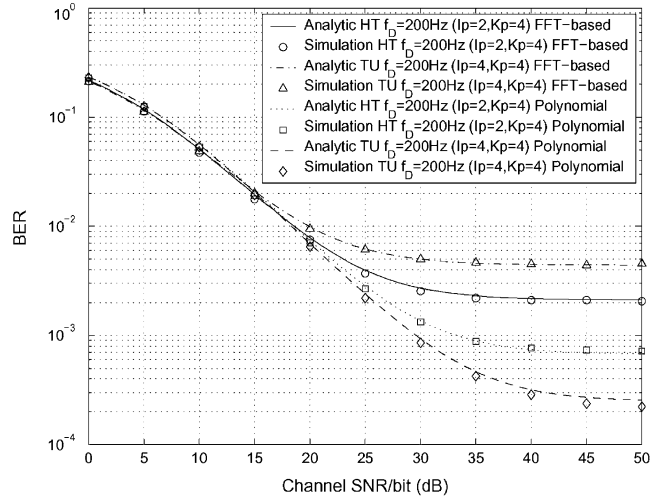
A. Comparison for Data Transmission

As explained in Section IV, the FFT-based channel estimation suffers from the leakage effect when the delay paths are not separated by integer multiples of the sampling period. The leakage effect, which causes severe performance degradation in FFT-based schemes, cannot be eliminated by increasing the channel SNR or the density of training pilots. The polynomial-based channel estimation does not have the leakage effect and performs very well as long as the channel frequency response in the approximation window changes smoothly. This can be ensured by choosing small approximation window and increasing pilot density.

We first compare both channel estimation methods for data transmission. The setup of the OFDM modulation is the same as that in Section III-D. The pilot spacing $(I_p, K_p) = (4, 4)$ is chosen for the TU delay profile, and $(I_p, K_p) = (2, 4)$ is chosen for the HT delay profile. In the FFT-based method, the degree of Lagrange interpolator is $L_{deg} = 3$. According to the maximum delay spread and the total bandwidth, the parameter K_0 is 5 for the TU delay and is 15 for the HT delay. In the polynomial-based method, the polynomial degrees are chosen as $I_{deg} = J_{deg} = 3$.

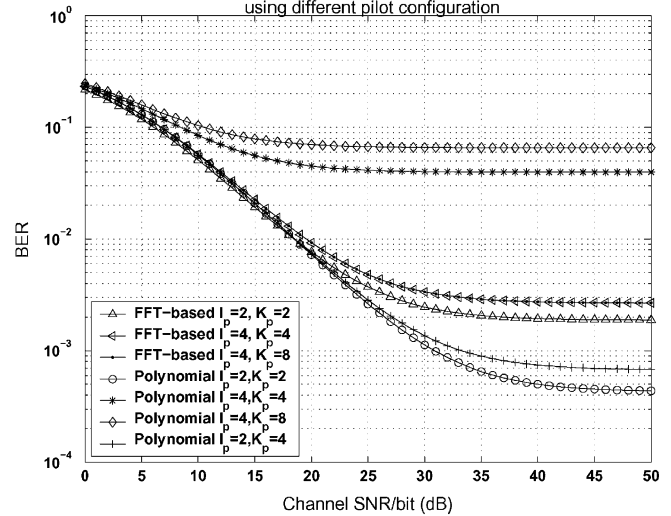
Fig. 12(a) shows the analytical and simulated BER performance for both channel estimation schemes. The simulation results are obtained by transmitting 24 000 OFDM blocks, and the BER shown in the figure represents the average performance of all subchannels. The analytical BER is evaluated by using the channel estimation MSE derived in Sections III-B and IV-B and the results in [29]. From the figure, we observe that the FFT-based channel estimation has an error floor in all channel conditions, due to the leakage effect. The polynomial-based channel estimation achieves lower BER, although it also has

Performance Comparison FFT based and polynomial based channel estimation



(a)

Performance of channel estimation schemes in HT delay profile, $f_D=200$ Hz using different pilot configuration



(b)

Fig. 12. Comparison between FFT- and polynomial-based methods. (a) $f_D = 200$ Hz. (b) HT delay, $f_D = 200$ Hz.

the error floor in the TU-200 and HT-200 cases, due to the model errors. In addition, the FFT-based method has slightly better performance in the low-channel SNR region. This is because that the FFT-based methods can remove the channel noise by eliminating the high-frequency components when performing IFFT-FFT filtering. In moderate and high SNR regions, removing high-frequency components causes model error since the energy of the channel frequency response spread over all the frequency bins due to the leakage effect. Thus, the polynomial-based method performs much better than the FFT-based method in moderate and high SNR regions.

We also investigate the effects that the pilot density has on these two channel estimation schemes in Fig. 12. It is important to point out that IFFT-FFT filtering is suitable for interpolating sinusoidal like functions, whereas polynomial interpolation is suitable for slow-varying functions. In some situations, the polynomial-based method needs more pilots than

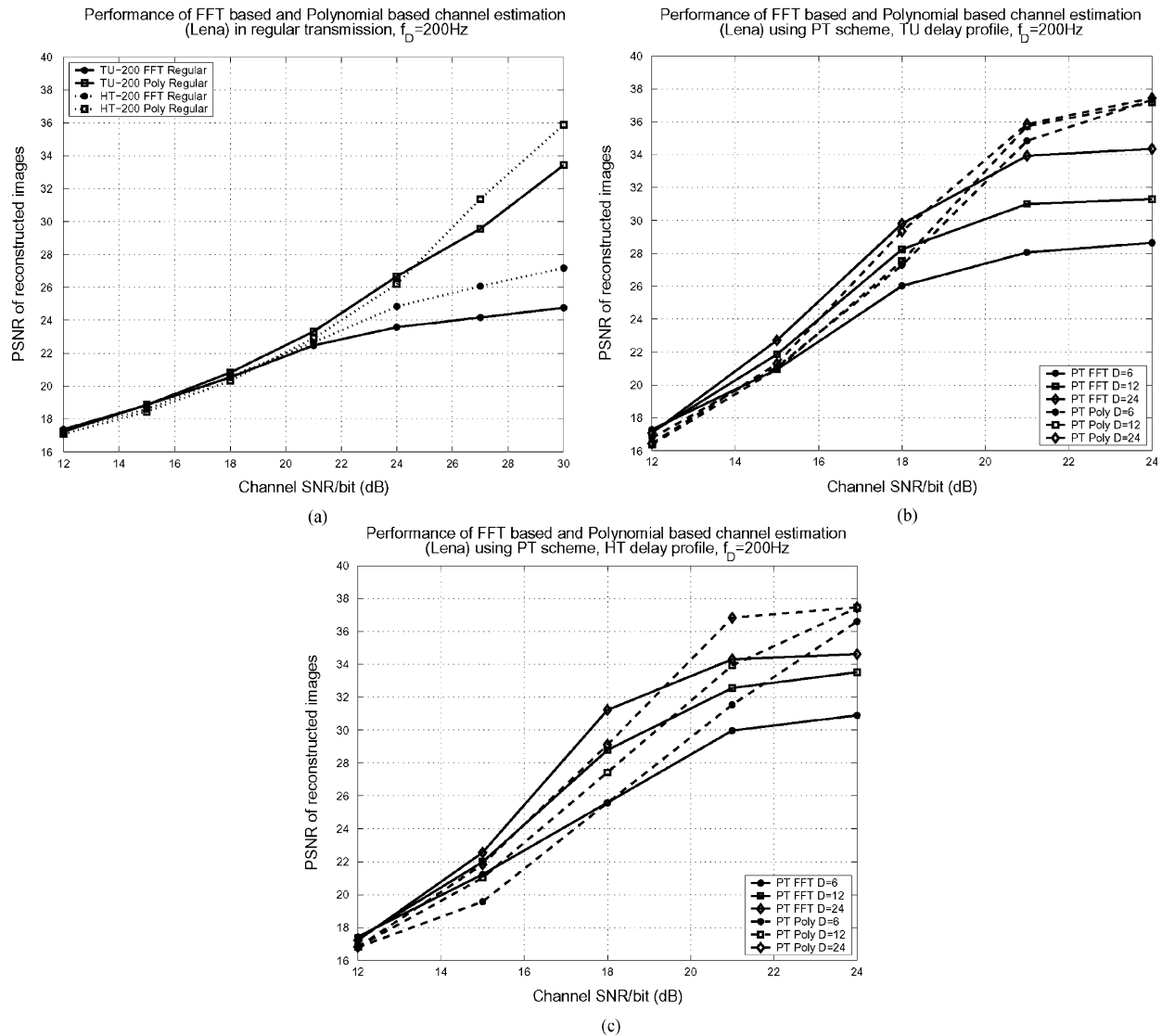


Fig. 13. Comparison of PT schemes in FFT- and polynomial-based channel estimation for image transmission. For HT, $(I_p, K_p) = (2, 4)$, and TU $(I_p, K_p) = (4, 4)$. (a) Comparison between FFT- and polynomial-based methods in regular transmission. (b) Comparison between FFT- and polynomial-based methods with the PT scheme in TU delay. (c) Comparison between FFT- and polynomial-based methods with the PT scheme in HT delay.

the FFT-based method to achieve good performance. For instance, in the HT-200 channel with pilot spacing $I_p = K_p = 4$, the FFT-based method has better performance than the polynomial-based method. This is because the polynomial basis cannot accurately model fast changing sinusoidal functions along different subchannels, as in the HT delay scenario, within a large approximation window. In this case, the approximation window size should be reduced.

In summary, the polynomial-based channel estimation outperforms the FFT-based channel estimation for data transmission in the realistic channel SNR region when pilot density is large enough such that the channel frequency response within an approximation window can be modeled as 2-D polynomial functions.

B. Comparison for Multimedia Transmission

In this section, we study which channel estimation scheme is better for multimedia transmission. In Fig. 13(a), the average PSNR of reconstructed images with *Interleave 1* with

$D = 1$ (regular transmission) for the FFT-based and the polynomial-based methods are compared in TU and HT delay scenarios. Similar to the data transmission results, the polynomial-based method outperforms the FFT-based method in moderate and high SNR regions. In Fig. 13(b) and (c), these two channel estimation schemes are compared when the PT is employed. When the channel SNR is from 12 to 19 dB, the polynomial-based method is slightly worse than the FFT-based method, since the latter method can remove noise more effectively. When the channel SNR is higher, the polynomial-based method achieves better performance because the effects of the polynomial model error are much less pronounced than the leakage effect. In fact, these two channel estimation schemes have close performance since the PT scheme compensates for the imperfection of channel estimation.

C. Complexity Comparison

The complexity of the two channel estimation algorithms are compared in terms of the number of real additions and real mul-

TABLE I
COMPLEXITY COMPARISON: FFT VERSUS POLYNOMIAL BASED
METHOD PER OFDM BLOCK

Algorithm Complexity	FFT based	Polynomial
# Real Multiplications	$(1 + \frac{L_{deg}+1}{K})N \log_2 N + 2(K_0+1)(L_{deg}+1) + \frac{2N(J_{deg}+1)}{K I_p}$	$2N(J_{deg}+1)(1 + \frac{(J_{deg}+1)}{K}) + \frac{2N(J_{deg}+1)(L_{deg}+1)}{K I}$
# Real Additions	$2(1 + \frac{L_{deg}+1}{K})N \log_2 N + 2(K_0+1)L_{deg}$	$2N \frac{J_{deg}+(J_{deg}+1)L_{deg}}{K}$

tuplications needed to perform channel estimation per OFDM block. Let N denote the number of subchannels, I_p and K_p denote the pilot spacing, and $K = K_p \times L_{deg} + 1 = K_p \times J_{deg} + 1$ and $I = I_p \times I_{deg} + 1$ be the window size of the interpolation, where L_{deg} , I_{deg} , J_{deg} are the Lagrange interpolator degree and 2-D polynomial degree, respectively. Using these parameters, the complexity of both the algorithms are summarized in Table I. Assuming N is the power of two, the FFT operation requires $N \log_2 N$ real multiplications and $2N \log_2 N$ real additions [33]. The first term of the number of multiplication in FFT-based method corresponds to the IFFT-FFT pair, the second term corresponds to the Lagrange interpolation, and the third term corresponds to the process of finding the temporal estimate (8). Similarly, the first term in the number of addition corresponds to the IFFT-FFT operation, and the second term corresponds to the Lagrange interpolation. In complexity analysis for polynomial channel estimation, the terms $(\mathbf{Q}_{J_{deg}} \mathbf{q}_{I_{deg}}^\dagger)$ and $(\mathbf{Q}_{J_{deg}} \mathbf{q}_{I_{deg}}^\dagger)$ in (18) are assumed to be precomputed. The first term in the number of multiplications corresponds to the 2-D interpolation (18), and the second term corresponds to the process of finding temporal estimates. For instance, using simulation parameters in TU-200 in the previous sections, the FFT-based channel estimation requires 1240 multiplications and 2380 adders per OFDM block, whereas the polynomial method requires 1364 multiplications and 1005 adders per OFDM block. Therefore, the complexity of both channel estimation algorithms is comparable.

The additional computational complexity for performing *priority transmission* is described as follows. The PT scheme only requires matrix-matrix addition/multiplication to compute the channel estimation MSE, the sorting algorithm, and the estimation of channel correlation matrix. The estimation of the correlation matrix can be done using direct averaging of the channel frequency response products of the subchannels. This procedure will be done at the very initial of the transmission and can be continuously used afterward. It is important to notice that there are several OFDM transmitter design techniques that perform adaptive bit and power loading [32]. Typically, these methods require the eigenvalue decomposition of the channel correlation matrix, which may be infeasible when the number of OFDM subchannels are large. We note also the adaptive bit and power loading techniques also require the estimation of channel correlation matrix. Therefore, the PT scheme may be the method of choice in transmitting multimedia data.

VI. CONCLUSION

We present a Priority Transmission scheme that improves the performance of multimedia transmission by jointly considering the effects of channel estimation and the properties of multimedia. Depending on how much decoding delay the system can

afford, the PT scheme can outperform the transmission scheme without considering channel estimation effect (i.e., *Interleave 1* and *Interleave 2*) by more than 3 dB in the PSNR of reconstructed images. The gain obtained in the PT scheme comes from the fact that more important data are transmitted in the channels with less estimation error. This is implemented by rearranging the transmission order of multimedia according to the channel estimation error. As a result, the larger the decoding delay is, the higher flexibility exists in transmission reordering, and better performance can be obtained.

The proposed method works well with different channel estimation algorithms, namely, FFT- and polynomial-based channel estimation, as discussed in the paper. We compare the two types of channel estimation techniques and conclude that the polynomial channel estimation provides lower BER than the FFT-based channel estimation when the system cannot apply the PT scheme. On the other hand, when the system can apply the PT scheme, both FFT- and polynomial-based method provide comparably good results.

REFERENCES

- [1] *Radio Broadcasting Systems; Digital Audio Broadcasting (DAB) to Mobile, Portable and Fixed Receivers*, Mar. 1997.
- [2] *Digital Video Broadcasting (DVB) Framing Structure, Channel Coding and Modulation Digital Terrestrial television (DVB-T)*, Jun. 1999.
- [3] *Wireless LAN Medium Access Control (MAC) and Physical Layer (PHY) Specifications: High-Speed Physical Layers in the 5 GHz Band*, Sep. 1999.
- [4] J. Chuang and N. Sollenberger, "Beyond 3G: Waveband wireless data access based on OFDM and dynamic packet assignment," *IEEE Commun. Mag.*, vol. 38, no. 7, pp. 78–87, Jul. 2000.
- [5] L. J. Cimini Jr., "Analysis and simulation of a digital mobile channel using orthogonal frequency division multiplexing," *IEEE Trans. Commun.*, vol. 33, no. 7, pp. 665–675, Jul. 1985.
- [6] O. Edfors, J. J. van de Beek, S. K. Wilson, M. Sandell, and P. O. Borjesson, "OFDM channel estimation by singular value decomposition," *IEEE Trans. Commun.*, vol. 46, no. 7, pp. 931–939, Jul. 1998.
- [7] Y. G. Li, L. J. Cimini, and N. R. Sollenberger, "Robust channel estimation for OFDM systems with rapid dispersive fading channels," *IEEE Trans. Commun.*, vol. 46, no. 7, pp. 902–915, Jul. 1998.
- [8] J. J. van de Beek, O. Edfors, M. Sandell, S. K. Wilson, and P. O. Borjesson, "On channel estimation in OFDM systems," in *Proc. 45th IEEE Veh. Technol. Conf.*, Chicago, IL, Jul. 1999, pp. 815–819.
- [9] K. F. Lee and D. B. Williams, "Pilot-symbol-assisted channel estimation for space-time coded OFDM systems," *J. Applied Signal Process.*, vol. 2002, no. 5, pp. 507–516, May 2002.
- [10] Y. G. Li, "Pilot-symbol-aided channel estimation for OFDM in wireless systems," *IEEE Trans. Veh. Technol.*, vol. 49, no. 4, pp. 1207–1215, Jul. 2001.
- [11] C. Pandana, Y. Sun, and K. J. R. Liu, "Channel aware unequal error protection for image transmission over broadband wireless LAN," in *Proc. IEEE Int. Conf. Image Process.*, 2003, pp. 93–96.
- [12] Y. Sun, C. Pandana, X. Wang, and K. J. R. Liu, "A joint channel estimation and unequal error protection scheme for image transmission in wireless OFDM systems," in *Proc. IEEE Int. Workshop Multimedia Signal Process.*, 2002, pp. 380–383.
- [13] A. Said and W. A. Pearlman, "A new, fast, and efficient image codec based on set partitioning in hierarchical trees," *IEEE Trans. Circuits Syst. Video Technol.*, vol. 6, no. 3, pp. 243–250, Jun. 1996.
- [14] M.-X. Chang and Y. T. Su, "Model-based channel estimation for OFDM signals in Rayleigh fading," *IEEE Trans. Commun.*, vol. 50, no. 4, pp. 540–544, Apr. 2002.
- [15] X. Wang and K. J. R. Liu, "An adaptive channel estimation algorithm using time-frequency polynomial model for OFDM," *J. Applied Signal Process.*, pp. 818–830, 2002.
- [16] —, "Channel estimation for multicarrier modulation systems using a time-frequency polynomial model," *IEEE Trans. Commun.*, vol. 50, no. 7, pp. 1045–1048, Jul. 2002.

- [17] M. Morelli and U. Mengali, "A comparison of pilot-aided channel estimation methods for OFDM systems," *IEEE Trans. Signal Process.*, vol. 49, no. 12, pp. 3065–3073, Dec. 2001.
- [18] J. G. Proakis, *Digital Communications*, Third ed. Englewood Cliffs, NJ: Prentice-Hall, 1995.
- [19] R. Steele, *Mobile Radio Communications*. New York: IEEE, 1992.
- [20] W. C. Jakes, *Microwave Mobile Communications*. New York: Wiley, 1974.
- [21] P. Hoher, S. Kaiser, and P. Robertson, "Pilot-symbol aided channel estimation in time and frequency," in *Proc. IEEE Global Telecomm. Conf.*, Phoenix, AZ, Nov. 1997, pp. 90–96.
- [22] —, "Two-dimensional pilot-symbol-aided channel estimation by Wiener filtering," in *Proc. 1997 IEEE ICASSP*, Munich, Germany, Apr. 1997, pp. 1845–1848.
- [23] A. A. Alatan, M. Zhao, and A. N. Akansu, "Unequal error protection of SPIHT encoded image bit streams," *IEEE J. Sel. Areas Commun.*, vol. 18, no. 6, pp. 814–818, Jun. 2000.
- [24] C. W. Yap and K. N. Ngan, "Error resilient transmission of SPIHT coded images over fading channels," in *Proc. Inst. Elect. Eng. Vision, Image, Signal Process.*, vol. 148, Feb. 2001, pp. 59–64.
- [25] P. A. Bello, "Characterization of randomly time-variant linear channels," *IEEE Trans. Commun.*, vol. COMM-11, no. 4, pp. 360–393, Dec. 1963.
- [26] A. K. Jain, *Fundamentals of Digital Image Processing*. Englewood Cliffs, NJ: Prentice-Hall, 1989.
- [27] Y. G. Li, N. Seshadri, and S. Ariyavisitakul, "Channel estimation for OFDM systems with transmitter diversity in mobile wireless channels," *IEEE J. Select. Areas Commun.*, vol. 17, no. 3, pp. 461–471, Mar. 1999.
- [28] X. Tang, M.-S. Alouini, and A. J. Goldsmith, "Effect of channel estimation error on M-QAM ber performance in Rayleigh fading," *IEEE Trans. Commun.*, vol. 47, no. 12, pp. 1856–1864, Dec. 1999.
- [29] M.-X. Chang and Y. T. Su, "Performance analysis of equalized OFDM systems in Rayleigh fading," *IEEE Trans. Wireless Commun.*, vol. 1, no. 4, pp. 721–732, Oct. 2002.
- [30] S. Lin and D. J. Costello Jr., *Error Control Coding: Fundamentals and Applications*. Englewood Cliffs, NJ: Prentice-Hall, 1983.
- [31] I. S. Reed and X. Chen, *Error Control Coding for Data Networks*. Boston, MA: Kluwer, 1999.
- [32] S. Zhou and G. B. Giannakis, "Optimal transmitter Eigen-beamforming and space-time block coding based on channel correlations," *IEEE Trans. Inf. Theory*, vol. 49, no. 7, pp. 1673–1690, Jul. 2003.
- [33] A. V. Oppenheim and R. W. Schaffer, *Discrete-time Signal Processing*. Englewood Cliffs, NJ: Prentice-Hall, 1989.



Charles Pandana was born in Indonesia. He received the B.S. and M.S. degrees in electronics engineering from the National Chiao Tung University, Hsinchu, Taiwan, R.O.C., in 1998 and 2000, respectively. He is currently pursuing the Ph.D. degree in electrical and computer engineering with the Department at the University of Maryland, College Park.

His research interests lie in the stochastic modeling/learning and channel estimation in broadband communications. He represented the Indonesia

National Team in the International Mathematics Olympiad and International Physics Olympiad in 1993 and 1994, respectively.



Yan Sun received the B.S. degree with the highest honor from Beijing University, Beijing, China, in 1998 and the Ph.D. degree in electrical and computer engineering from the University of Maryland, College Park, in 2004.

She is currently an NSF ADVANCE assistant professor with the Electrical and Computer Engineering Department, University of Rhode Island, Kingston. Her research interests include network security and wireless communications and networking.

Dr. Sun received the Graduate School Fellowship at the University of Maryland from 1998 to 1999 and the Excellent Graduate Award of Beijing University in 1998. She is a member of the IEEE Signal Processing and Communication Societies.



K. J. Ray Liu (F'03) received the B.S. degree from the National Taiwan University, Taipei, Taiwan, R.O.C., in 1983 and the Ph.D. degree from the University of California, Los Angeles, in 1990, both in electrical engineering.

He is Professor and Director of the Communications and Signal Processing Laboratories of the Electrical and Computer Engineering Department and Institute for Systems Research, University of Maryland, College Park. His research contributions encompass broad aspects of wireless communications and networking; information forensics and security; multimedia communications and signal processing; signal processing algorithms and architectures; and bioinformatics, in which he has published over 350 refereed papers.

Dr. Liu is the recipient of numerous honors and awards, including the IEEE Signal Processing Society 2004 Distinguished Lecturer, the 1994 National Science Foundation Young Investigator Award, the IEEE Signal Processing Society's 1993 Senior Award (Best Paper Award), and the IEEE 50th Vehicular Technology Conference Best Paper Award (Amsterdam, The Netherlands, 1999), and the EURASIP 2004 Meritorious Service Award. He received the 2005 Poole and Kent Senior Faculty Teaching Award from the A. James Clark School of Engineering, University of Maryland, as well as the George Corcoran Award in 1994 for outstanding contributions to electrical engineering education and the Outstanding Systems Engineering Faculty Award in 1996 in recognition of outstanding contributions in interdisciplinary research, both from the Institute for Systems Research. He is the Editor-in-Chief of the IEEE SIGNAL PROCESSING MAGAZINE, the prime proposer and architect of the new IEEE TRANSACTIONS ON INFORMATION FORENSICS AND SECURITY, and was the founding Editor-in-Chief of the *EURASIP Journal on Applied Signal Processing*. He is a Board of Governor at large of the IEEE Signal Processing Society.